Eur. Phys. J. D **3**, 275–288 (1998)

THE EUROPEAN PHYSICAL JOURNAL D

Transverse dynamics of optical parametric oscillators in presence of walk-off

H. Ward[1], M.N. Ouarzazi[2], M. Taki[1,a], and P. Glorieux[1]

[1] Laboratoire de Physique des Lasers, Atomes et Molécules[b], Centre d'Études et de Recherches Lasers et Applications, Université des Sciences et Technologies de Lille, 59655 Villeneuve d'Ascq Cedex, France
[2] Laboratoire de Mécanique de Lille[b], Université des Sciences et Technologies de Lille, 59655 Villeneuve d'Ascq Cedex, France

Received: 4 March 1998 / Revised: 15 June 1998 / Accepted: 23 June 1998

Abstract. We present a model for non degenerate optical parametric oscillators (OPO) including diffraction and walk-off effects, and report how the transverse beam profile is changed by the walk-off. A complex order-parameter description for the OPO near threshold leads to a two dimensional evolution equation with symmetry breaking stemming from the presence of walk-off. We find that the onset of instability is hastened and that the emerging transverse beam profile propagates in the walk-off direction. This prediction agrees qualitatively with recent experimental results. The convective nature of the instability at the first bifurcation predicts that only the noise-sustained structures may play an important role. The absolute instability observed at larger values of the pump parameter, gives rise to dynamically self-sustained patterns. Numerical simulations are reported to illustrate a possible sequence of convective and absolute instabilities together with the subsequent nonlinear transverse spatio-temporal dynamics.

PACS. 42.65.Yj Optical parametric oscillators and amplifiers – 42.65.Sf Optical spatio-temporal dynamics – 47.20.-k Hydrodynamic stability

1 Introduction

Together with stimulated emission, parametric amplification is a fundamental mechanism for generation of coherent radiation. The former is the basis of laser action and the latter that of optical parametric oscillation. On the one hand, laser theory has been the subject of intense activity and there are now very sophisticated theories for a wide variety of lasers. Lasers are now well understood and widely used in many different fields but on the other hand optical parametric oscillators are less known. In fact, although the basic process of optical parametric amplification has been discovered more than 30 years ago, Optical Parametric Oscillators (OPO) developed quickly only in the last ten years mostly for technological reasons [1]. Compared to lasers, OPOs have received much less attention in spite of their strong interest both on the fundamental and on the technological sides [2].

Let us recall that these are very frequency agile coherent sources with a wide range of possible applications including range finding, pollution monitoring and tunable frequency generation... They are also the key element for the production of twin photons and the realization of fundamental quantum optics experiments [3].

Basically an optical parametric amplifier generates light *via* a three-wave mixing process in which a nonlinear crystal subjected to a strong radiation at frequency ω_p (pump beam) radiates two coherent fields at frequencies ω_s(signal beam) and ω_i (idler beam) such that the energy conservation law

$$\omega_p = \omega_s + \omega_i$$

is satisfied. This energy conservation criterion may be interpreted in terms of photons where one photon at frequency ω_p is converted into two photons at frequencies ω_s and ω_i. This process is most efficient when the phase matching condition is fulfilled. It states that optical parametric amplification is favored when the three interacting waves keep constant relative phases along their propagation inside the crystal. This implies

$$\mathbf{k}_p = \mathbf{k}_s + \mathbf{k}_i,$$

or equivalently

$$n_p(\omega_p)\omega_p = n_s\left(\omega_s\right)\omega_s + n_i\left(\omega_i\right)\omega_i$$

where k_j and n_j are the wavevector and the refractive index at frequency ω_j respectively ($j = p, s, i$).

It is classical to compensate for the unavoidable material chromatic dispersion, *i.e.* its refractive index variation with frequency, by taking advantage of the crystal

[a] e-mail: majid.taki@univ-lille1.fr
[b] Laboratoire associé au CNRS.

birefringence. In birefringent crystals, the refractive index depends on the polarization state and using different polarizations for the beams it is possible to match their phase velocities. Several configurations are encountered depending on which wave propagates along an ordinary or an extraordinary axis of the crystal. Typical configurations are the type I and type II phase-matching. In type I the signal and idler beams are ordinary (extraordinary) waves while in type II one is ordinary and the other one is extraordinary and the pump is extraordinary (ordinary) in negative (positive) crystals for both. As the extraordinary index depends on the propagation direction, the phase matching condition is angle dependent. For instance for type I phase matching in a positive crystal, it writes

$$n_p^o(\omega_p)\omega_p = n_s^e(\omega_s,\theta)\omega_s + n_i^e(\omega_i,\theta)\omega_i$$

where superscripts e and o refer to extraordinary and ordinary waves respectively. For any angle $\theta \in \left]0, \frac{\pi}{2}\right[$ the Poynting vector and the wavevectors $\mathbf{k}$ are not parallel. As a result even ordinary and extraordinary rays with parallel wavevectors have different Poynting vector directions and therefore the rays diverge from one another as they propagate through the birefringent medium. This is the so called walk-off effect which limits the overlap of the waves and imposes severe restrictions on the efficiency of optical parametric amplification.

As for a laser, the active medium of the OPO is placed inside an optical cavity which ensures optical feedback and enhances the interaction. Most theories of OPOs are developed in the mean field limit in which the electric field distribution is uniform inside the laser cavity. Recently Longhi [4] extended the mean field laser theory of Lega *et al.* [5] to OPOs. In this approach, diffraction of the beams is included, introducing some transverse dependence of the variables. This results in a problem much more complicated than standard laser models because the transverse dependence of the variables changes the Haken-Lorenz equations of the laser into a partial differential equation system which requires more sophisticated treatments both analytically and numerically. However, in mean field theories the longitudinal dependence of the variables is neglected, this is valid for single mode operation, no pump depletion and a short cavity almost filled by the crystal. There has recently been significant improvements of the OPO theory including simultaneously transverse effects and propagation along the cavity axis [6]. The work developed here considers the walk-off effect but does not include longitudinal effects and therefore is not relevant for high gain situations in which the energy transfer from the pump beam to the signal and idler is efficient in a single-pass.

From an intuitive point of view, it is clear that walk-off effects should alter the properties of pattern formation in the OPOs. Because the different interacting rays do not propagate exactly in the same direction, symmetry is broken by the walk-off effect and new patterns are expected. Recent experiments [7] exhibited clearly the transverse dependence [8] of the optical beams in optical parametric amplification. They demonstrated that the beams expand transversely in the walk-off direction [9]. It is crucial to elucidate the mechanisms underlying these phenomena and in particular to separate noise-induced patterns from those originating from the intrinsic dynamics of the system. This optical situation is analogous to that encountered in Rayleigh-Bénard convection in presence of a transverse flow as it was experimentally studied by Ouazzani *et al.* [10]. Müller *et al.* [11] discussed the structure and the nature of the solutions of this problem. They showed that a small lateral through flow stabilizes the conductive state and described the effect of this flow upon the competition between transverse and longitudinal rolls. This has recently been extended to Rayleigh-Bénard convection in a porous medium with qualitatively similar results [12]. Just like for these perturbed instabilities, the most interesting cases in OPOs occur when the symmetry-breaking term is weak enough to allow pattern formation but not too weak to be negligible. This is exactly the case of the walk-off effect since for almost all experimental situations the walk-off angle is $\varrho \simeq 3^\circ$ for phase-matching angle $\theta \simeq 45^\circ$. The difference between convective and absolute instabilities which proved its efficiency in the theory of hydrodynamic instabilities [13] is extensively used in the present work. In particular we show that the two kinds of instabilities have different impacts on the OPO efficiency.

In spite of its common points with the Rayleigh-Bénard problem and the laser, the OPOs have some specificities with respect to both problems. The differences with Rayleigh-Bénard convection are obvious and do not need further comment. The main differences with the laser lie in the nature of the light-matter interaction. As far as modelization is concerned, the OPOs have the great advantage of a very simple and exact description of the interaction by a quadratic term involving only electric fields and no matter variables. Moreover the OPOs offer a large variety of configurations due to the three radiations involved in the parametric process. The optical cavities that must be used for efficient coupling of these fields may be simply, doubly and triply resonant, *i.e.* may resonate with one, two of the three or the three fields, contrarily to lasers in which only one resonant electric field builds up. Therefore the OPO has a much wider parameter space than the laser.

The paper is organized in the following way. In the next section we present the basis of the model and the governing equations for the OPOs in presence of walk-off and diffraction effects. In Section 3 an evolution equation is derived which we expect to be relevant for the real OPO system in the weakly nonlinear regime close to threshold. A spatio-temporal stability analysis has been carried out in Section 4 to determine whether a pattern becomes convectively or absolutely unstable and to evaluate the corresponding threshold instabilities. We end up in Section 5 by pointing out that some of our analytical and numerical results are in qualitative agreement with corresponding experimental works.

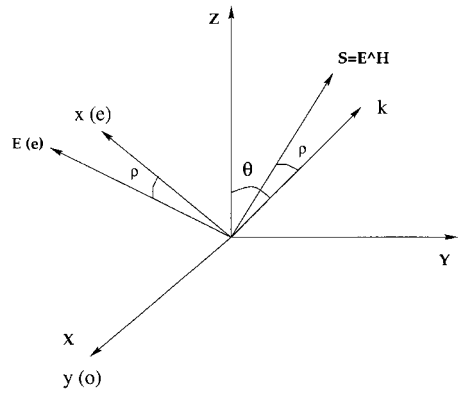

Fig. 1. Crystallographic coordinate system (X,Y,Z) and laboratory coordinate system (x,y,z). θ indicates the phase matching angle between the crystal optical Z axis and the longitudinal direction of wave propagation $\mathbf{k}$. (o) and (e) stand for ordinary and extraordinary, respectively. The walk-off angle ρ corresponding to a tilt of the Poynting vector direction $\mathbf{S}$ with respect to the direction of wave propagation $\mathbf{k}$, and the extraordinary electric field E (e) are also shown.

2 Theoretical model

In this section, we construct a model for optical parametric oscillators including diffraction and walk-off effects. First we recall the modified paraxial wave equations that describe propagation in an uniaxial crystal. Due to the walk-off effect, the Poynting vector for waves with extraordinary polarization propagates with a small angle ρ relative to its wavevector $\mathbf{k}$ contrarily to ordinary waves for which the Poynting vector and the wavevector are parallel. The model is then extended to take into account the optical cavities which we are interested in, within the mean field limit.

2.1 Maxwell wave equation in presence of walk-off

For wave propagation in an anisotropic crystal, it is necessary to express the equations in two different coordinate systems, namely crystallographic coordinates (X, Y, Z) and laboratory coordinates (x, y, z). The wave propagates along the direction z which is tilted by an angle θ from the optical axis Z of the crystal (see Fig. 1). The unit vector components in the first system are denoted by $(\mathbf{e}_1, \mathbf{e}_2, \mathbf{e}_3)$ while those of the second one are denoted by $(\mathbf{e}, \mathbf{o}, \mathbf{z})$. In the last notation which is more convenient as it will be seen in the following, $\mathbf{z}$ is the unit vector along propagation direction $\mathbf{k}$, and $\mathbf{e}$ and $\mathbf{o}$ are the unit vectors along extraordinary and ordinary polarization directions for the waves considered in this problem. Anticipating on the classical properties of light propagation in uniaxial crystals we choose to have y coincident with the X axis.

The laboratory coordinate axes are simply obtained by a rotation through an angle $\frac{\pi}{2} - \theta$ about x axis. The two coordinate systems are related by

$$\begin{aligned} x &= -Y\cos\theta + Z\sin\theta \\ y &= X \\ z &= Y\sin\theta + Z\cos\theta. \end{aligned} \tag{1}$$

Our starting point is the Maxwell wave equation for nonconducting and nonmagnetic media

$$\triangle\mathbf{E} - \nabla(\nabla.\mathbf{E}) - \mu_0\frac{\partial^2\mathbf{D}}{\partial t^2} = 0, \tag{2}$$

where $\mathbf{E}$ is the electromagnetic field, $\mathbf{D} = \varepsilon_0\varepsilon_r \cdot \mathbf{E} + \mathbf{P}_{NL}$ is the electric displacement vector written as a sum of the linear and nonlinear terms and ε_r represents the usual relative permittivity tensor. For an uniaxial crystal ε_r takes a diagonal form in the crystallographic coordinates whose eigenvalues are $\varepsilon_1 = \varepsilon_2 = n_0^2$ and $\varepsilon_3 = n_e^2$ where n_0 and n_e are the ordinary and the extraordinary refractive indices respectively.

By setting

$$\mathbf{E} = \boldsymbol{\xi}(t, z, x, y)\exp\left[-i(\omega t - k_0 n z)\right] \tag{3}$$

in the expression of $\mathbf{D}$ and substituting it into equation (2) we obtain, after straightforward calculations, the following equation:

$$\triangle\mathbf{E} - (1-\gamma^2)\nabla\left(\frac{\partial E_3}{\partial Z}\right) - \frac{1}{c^2}\frac{\partial^2(\varepsilon_r \cdot \mathbf{E})}{\partial t^2} - \mu_0\frac{\partial^2\mathbf{P}_{NL}}{\partial t^2} = 0, \tag{4}$$

where $\gamma^2 = n_e^2/n_0^2$ and $c = \omega/k_0$. Notice that the second term in equation (4) is specific of the crystal anisotropy. It states that, contrary to isotropic media, the electric field is generally not transverse to the direction of wave propagation (see Fig. 1). The nonvanishing E_3 component gives rise to a walk-off angle for the power propagation with respect to wave propagation. The importance of the power walk-off is directly proportional to the crystal birefringence $\Delta n = n_e - n_0$ as can be seen from the coefficient of the second term in equation (4).

2.2 Basic equations for OPOs: Free and optical cavity propagation

So far we have not specified the nonlinear terms for the propagating beams in the crystal. In fact the parametric process requires the resonance relation $\omega_p = \omega_s + \omega_i$ and the process is optimized under the phase-matching relation $\mathbf{k}_p = \mathbf{k}_s + \mathbf{k}_i$, where the subscripts p, s and i refer to the pump, signal and idler respectively. In all what follows we consider a positive crystal ($n_e > n_0$), and a general situation where two of the beams are extraordinary waves experiencing the walk-off effect. Therefore when the idler is ordinary we recover the experimental situation considered by Smith *et al.* [8] while for an ordinary signal we meet conditions for the experimental study of Nishikawa

and Uesugi [9]. We assume here the following phase-matching: $\mathbf{k}_{p,(o)} = \mathbf{k}_{s,(e)}(\theta) + \mathbf{k}_{i,(e)}(\theta)$ which means that the signal and idler are extraordinary beams, polarized in the principal plane x, z while the pump is an ordinary beam polarized in the direction y perpendicular to the principal plane.

We emphasize that the case of negative crystals can be treated straightforwardly by following our analysis and setting the pump as an extraordinary beam while either the signal or the idler is an ordinary beam. Thus the following analysis gives a general framework in which it is possible to consider all types of phase matching for both positive and negative crystals.

Since in almost all OPO systems the nonlinear interaction is local and instantaneous with dominant quadratic $\chi^{(2)}$ effects, we assume $\mathbf{P}_{NL} = \varepsilon_0 \chi^{(2)} |\mathbf{E} : \mathbf{E}|$.

In this situation and with the help of equation (4) written for an extraordinary (ordinary) beam, the nonlinear interaction of the three waves propagating in the crystal is governed by the system:

$$\begin{aligned}
\frac{\partial \xi_p}{\partial z} + \frac{n_0}{c}\frac{\partial \xi_p}{\partial t} &= \frac{i}{2k_p}\triangle_\perp \xi_p + i\frac{\omega_p}{n_0 c} d_{eff}\xi_s \xi_i \exp[-i(\Delta k)z] \\
\frac{\partial \xi_s}{\partial z} + \frac{n_s}{c}\frac{\partial \xi_s}{\partial t} &= \frac{i}{2k_s}\triangle_\perp \xi_s - \tan\varrho_s \frac{\partial \xi_s}{\partial x} + i\frac{\omega_s}{n_s c} d_{eff}\xi_p \xi_i^* \\
&\quad \times \exp[i(\Delta k)z] \\
\frac{\partial \xi_i}{\partial z} + \frac{n_i}{c}\frac{\partial \xi_i}{\partial t} &= \frac{i}{2k_i}\triangle_\perp \xi_i - \tan\varrho_i \frac{\partial \xi_i}{\partial x} + i\frac{\omega_i}{n_i c} d_{eff}\xi_p \xi_s^* \\
&\quad \times \exp[i(\Delta k)z], \qquad (5)
\end{aligned}$$

where ξ_p, ξ_s and ξ_i are the envelopes of the pump, the signal and the idler respectively, and n_0, n_s, n_i are the refractive indices of the pump, signal and idler fields respectively. We have set $\chi^{(2)} = 2d_{eff}$ and $\Delta k = |\mathbf{k}_p - \mathbf{k}_s - \mathbf{k}_i|_z$ to account for a possible mismatch. The walk-off angle $\varrho_{s(i)}$ is related to the phase matching angle $\theta_{s(i)}$ by the relation $\tan\varrho_{s(i)} = \tau_{s(i)}/\beta^2_{s(i)}$ where $2\tau_{s(i)} = (\gamma^2 - 1) \times \sin(2\theta_{s(i)})$ and $\beta^2_{s(i)} = \gamma^2 \cos^2\theta_{s(i)} + \sin^2\theta_{s(i)}$, and $\triangle_\perp$ is the Laplacian acting on the transverse coordinates x and y. Note that $\tan\varrho_{s(i)}$ is a small parameter which is typically of the order of the crystal birefringence $\Delta n = n_e - n_0$. This justifies the fact that the walk-off is taken as a small parameter in the following study. The above plane polarized beam assumption is consistent with the paraxial approximation, and constitutes a good approximation so long as the directions of the two wave components in the beam do not deviate much from the direction of propagation. We have also neglected in equations (5) the slight asymmetry of diffraction in the transverse variables (due to the crystal birefringence) with respect to the walk-off effect.

The relevance of this model has already been tested by several authors. Among those who included walk-off, one should mention Smith *et al.* [8] and Nishikawa and Uesugi [9] (diffraction has been neglected by the last authors) who integrated numerically equations (5) and both groups obtained results in a very good agreement with the experiments. Analytical treatment is also possible and it is interesting to explore the possibilities of this approach compared to the extensive experimental and numerical investigation which has been carried out in the above mentioned references.

However, in order to keep the analysis as simple as possible to get more insight into the role of the walk-off in the transverse dynamics, we will extend the model to take into account optical cavities with large aspect ratio but we restrict ourselves to single longitudinal mode OPOs. Assuming that the cavity is triply resonant, one may reduce equations (5) by means of the mean-field limit approximation. Since the procedure is well known and detailed calculations are similar to that of reference [16] we do not repeat them here. After lengthy but straightforward calculations, equations (5) are transformed into:

$$\begin{aligned}
\partial_t A_p &= \gamma_p[-(1 + i\Delta_p)A_p + ia_p\triangle_\perp A_p - A_s A_i + E(x,y)] \\
\partial_t A_s &= \gamma_s[-(1 + i\Delta_s)A_s + ia_s\triangle_\perp A_s + A_p A_i^* - \alpha_s \partial_x A_s] \\
\partial_t A_i &= \gamma_i[-(1 + i\Delta_i)A_i + ia_i\triangle_\perp A_i + A_p A_s^* - \alpha_i \partial_x A_i] \qquad (6)
\end{aligned}$$

where A_p, A_s, and A_i, are the adimensional complex envelopes of the pump, signal and idler fields respectively and $E(x,y)$ is the external normalized pump signal. Note that these envelopes are expressed in terms of the transformed variables for which the longitudinal boundary conditions of the cavity are homogeneous, as is customary in the mean-field limit (see Ref. [16]). Δ_p, Δ_s, and Δ_i are three detuning parameters for pump, signal and idler fields, respectively, defined by $\Delta_p = (\omega_0 - \omega_p)/\gamma_p$, $\Delta_s = (\omega_1 - \omega_s)/\gamma_s$, $\Delta_i = (\omega_2 - \omega_i)/\gamma_i$, where γ_p, γ_s and γ_i are the cavity decay rates for the three fields, ω_0, ω_1, and ω_2 are the three cavity resonance frequencies closest to the pump frequency ω_p, the signal frequency ω_s, and the idler frequency ω_i, respectively. The diffraction parameters a_p, a_s, a_i are given by $a_p = c/(2n_0 k_p \gamma_p)$, $a_s = c/(2n_s k_s \gamma_s)$, $a_i = c/(2n_i k_i \gamma_i)$ where k_p, k_s and k_i are the longitudinal wave numbers of the pump, signal, and idler fields respectively. Finally in equations (6) the walk-off parameters are defined as $\alpha_s = c\tan\varrho_s/(n_s\gamma_s)$ and $\alpha_i = c\tan\varrho_i/(n_i\gamma_i)$ for the signal and idler fields respectively.

In the absence of walk-off ($\alpha_s = \alpha_i = 0$) we recover the set of governing equations of OPOs in optical cavities where transverse pattern formation has been investigated leading to either the appearance of rolls, filamentation and turbulence [17], traveling waves and standing waves [18] or the existence of optical defects [19]. The effect of walk-off on transverse pattern formation which acts as gradient term breaking the reflection symmetry has not been yet investigated. It is the main concern in the following.

3 Linear and nonlinear analysis in presence of walk-off

3.1 Neutral stability curve

The equations

$$\begin{aligned}\partial_t A_p &= \gamma_p[-(1+i\Delta_p)A_p + E(x,y) - A_s A_i + i a_p \Delta_\perp A_p]\\ \partial_t A_s &= \gamma_s[-(1+i\Delta_s)A_s + A_p A_i^* + i a_s \Delta_\perp A_s - \alpha_s \partial_x A_s]\\ \partial_t A_i &= \gamma_i[-(1+i\Delta_i)A_i + A_p A_s^* + i a_i \Delta_\perp A_i - \alpha_i \partial_x A_i] \end{aligned} \quad (7)$$

describing the dynamics of the pump, signal, and idler waves respectively, have a homogeneous and time-independent solution:

$$A_p = \frac{E}{1+i\,\Delta_p} \equiv \mu \quad A_s = 0 \quad A_i = 0. \quad (8)$$

It is convenient to write equations (7) in terms of the deviations from the equilibrium $B = A_p - \mu$, A_s, and A_i which obey the following system:

$$\begin{aligned}\partial_t B &= \gamma_p[-(1+i\Delta_p)B + i a_p \Delta_\perp B\,] - \gamma_p A_s A_i\\ \partial_t A_s &= \gamma_s[-(1+i\Delta_s)A_s + i a_s \Delta_\perp A_s + \mu A_i^* - \alpha_s \partial_x A_s]\\ &\quad + \gamma_s A_i^* B\\ \partial_t A_i^* &= \gamma_i[-(1-i\Delta_i)A_i^* - i a_i \Delta_\perp A_i^* + \mu A_s - \alpha_i \partial_x A_i^*]\\ &\quad + \gamma_i A_s B^*. \end{aligned} \quad (9)$$

We then proceed to a stability analysis by linearizing equations (9) around the basic state (8) and considering solutions of the form $\exp(ik_x x + ik_y y + \lambda t)$, where $\mathbf{k} = (k_x, k_y)$ is the transverse wave vector and λ is an eigenvalue of the linear problem.

As can be seen from equations (8, 9), the linear pump perturbations are decoupled from that of the signal and idler envelopes and thus the analysis reduces to the study of the linearized form of the two last equations of (9). One obtains after straightforward calculations the following characteristic equation for the signal and idler envelopes:

$$\lambda^2 - (b_s + b_i)\lambda + b_s b_i - \gamma_s \gamma_i \mu^2 = 0$$

where

$$\begin{aligned} b_s &= -\gamma_s[1 + i(\Delta_s + a_s k^2 + \alpha_s k_x)]\\ b_i &= -\gamma_i[1 - i(\Delta_i + a_i k^2 - \alpha_i k_x)]. \end{aligned}$$

The characteristic equation yields the neutral stability surface ($\mathrm{Re}(\lambda) = 0$) in the 2D plane of the wave vector components (k_x, k_y) in the form:

$$\begin{aligned}\omega &= \mathrm{Im}(\lambda)\\ &= \gamma_s\gamma_i[\Delta_s - \Delta_i + (a_s - a_i)k^2 - (\alpha_s + \alpha_i)k_x]/(\gamma_s + \gamma_i) \end{aligned} \quad (10)$$

$$\mu = \left(1 + (\Delta + ak^2 + \alpha k_x)^2/(\gamma_s + \gamma_i)^2\right)^{\frac{1}{2}} \quad (11)$$

where

$$\begin{aligned}\Delta &= \gamma_s\Delta_s + \gamma_i\Delta_i\\ a &= \gamma_s a_s + \gamma_i a_i\\ \alpha &= \gamma_s\alpha_s - \gamma_i\alpha_i. \end{aligned} \quad (12)$$

We start by recalling the problem without walk-off ($\alpha_s = \alpha_i = 0$) which has been recently studied by Longhi [4]. It immediately follows from equation (11) that minimizing μ with respect to k gives the instability threshold μ_c with critical wave number k_c and frequency ω_c. The value of these quantities depends on the sign of the "effective" detuning Δ. With $\Delta < 0$ the most unstable modes fall on a circle of magnitude $k_c = \sqrt{-\Delta/a}$ with a threshold given by $\mu_c = 1$ and $\omega_c = \omega(k_c)$ from equation (10). For $\Delta > 0$, criticality is obtained at $\mu_c = \sqrt{1+\tilde{\Delta}^2}$ with $\tilde{\Delta} = (\gamma_s\Delta_s + \gamma_i\Delta_i)/(\gamma_s + \gamma_i)$ and corresponds to an homogeneous state ($k_c = 0$) and associated frequency $\omega_c = \gamma_s\gamma_i(\Delta_s - \Delta_i)/(\gamma_s + \gamma_i)$. When the walk-off is present, the reflection symmetry $x \to -x$ in system (9) is broken. As pointed out above, this broken symmetry could introduce new bifurcation points and lead to new patterns. To understand this effect, we will mainly be focused on the case $\Delta > 0$, postponing the concerns of $\Delta < 0$ to later analyses. In this case, the gain parameter μ represents a surface which depends on the wave vector components (k_x, k_y) and cannot be reduced to a curve depending upon the modulus square k^2 as for standard ($\alpha_s = \alpha_i = 0$) OPOs when the rotational symmetry is preserved. By minimizing μ in equation (11) with respect to the wave vector $\mathbf{k} = (k_x, k_y)$ for positive nonvanishing "effective" detuning Δ, the instability threshold is reached, to leading order in α, for:

$$\mu = \sqrt{1+\tilde{\Delta}^2} - \alpha^2\Delta/\left[4a(\gamma_s + \gamma_i)^2\sqrt{1+\tilde{\Delta}^2}\right].$$

Perturbations that will first become unstable (*i.e.* whose wavevector minimizes threshold) are 1D structures expanding in the walk-off direction with $k_x^c = -\alpha/(2a)$ and $k_y^c = 0$. The relevant neutral stability curve (μ *versus* k_x) which corresponds to the projection of the neutral stability surface on the plane (μ, k_x) is reproduced in Figure 2. The neutral stability curve without walk-off is also shown for comparison. It clearly shows that the walk-off is responsible of the threshold lowering which is accompanied with a shift of the neutral stability curve towards negative or positive k_x depending on the sign of the "relative" walk-off α.

In addition to the above general situation, it is worthy to mention the particular case of the degenerate OPO systems where $\gamma_s = \gamma_i$, $a_s = a_i$, $\Delta_s = \Delta_i$ and $\alpha_s = \alpha_i$. As a consequence, the relative walk-off parameter α vanishes. The physical interpretation of this result is that the combined symmetric individual walk-off of the signal from one hand and the idler from the other hand results in a suppression of the relative walk-off effect. Thus, at threshold

$$L = \begin{pmatrix} -\gamma_p(1+i\Delta_p) + i\gamma_p a_p \Delta_\perp & 0 & 0 \\ 0 & -\gamma_s(1+i\Delta_s) + i\gamma_s a_s \Delta_\perp - \gamma_s \alpha_s \partial_x & \mu\gamma_s \\ 0 & \mu\gamma_i & -\gamma_i(1-i\Delta_i) - i\gamma_i a_i \Delta_\perp - \gamma_i \alpha_i \partial_x \end{pmatrix}$$

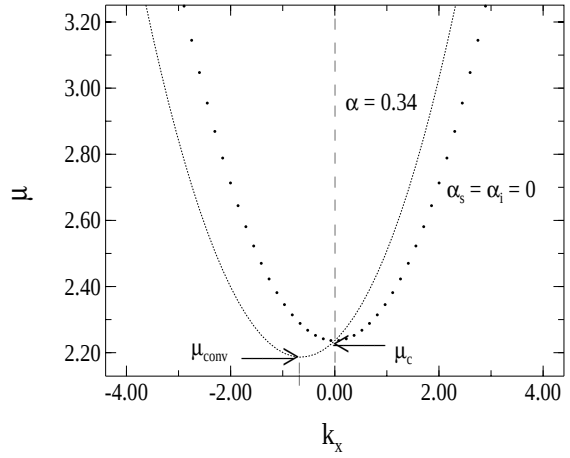

Fig. 2. Projection of the neutral stability surface $\mu = \mu(k_x, k_y)$ on the plane $(\mu,\ k_x)$ (dashed line) for $\alpha = 0.34$. Neutral stability curve in the absence of walk-off (dotted line) is also shown for reference. Note the lowering of the instability threshold from μ_c to μ_{conv} indicated by the arrows on the figure and the appearance of a unidimensional convective structure $k_x = \alpha/(\gamma_s a_s + \gamma_i a_i)$ and $k_y = 0$.

of instability, the situation is similar to that of absence of walk-off. In other words, the value of the gain parameter μ at the onset of instability and the most unstable mode remains unchanged ($\mu = \mu_c$ and $k = k_c = 0$). However, in spite of this significant difference between degenerate and non degenerate OPO systems, the walk-off influence is not reduced to the neutral stability curve. In addition, it can introduce a new phenomenon of power transport and affects both linear and nonlinear spatio-temporal dynamics. In order to understand the mechanisms of transverse pattern formation in this situation, a global-stability analysis in terms of convective and absolute instability [20] is required. In the remaining of the paper and for the clarity of the analysis we denote the value of the gain parameter, at the onset of instability, in the absence of walk-off by $\mu = \mu_c \equiv \sqrt{1+\tilde{\Delta}^2}$. When the walk-off is present, the new pump threshold at the onset of instability is termed $\mu = \mu_{conv} \equiv \mu_c - \alpha^2 \Delta / \left[4a(\gamma_s+\gamma_i)^2\sqrt{1+\tilde{\Delta}^2}\right]$.

3.2 Derivation of the modulation equation

In this subsection we base the nonlinear analysis on the outcome of the unperturbed ($\alpha_s = \alpha_i = 0$) linear stability analysis instead of fully analyzing the classical linearized stability problem by expanding the solutions as an asymptotic series in the small parameters α_s and α_i. Therefore, in the nonlinear stability theory we consider the nonlinear evolution of solutions of equations (9) for μ close to μ_c. We introduce another small parameter ε and the rescaled control parameter μ_2 given by

$$\mu - \mu_c = \varepsilon^2 \mu_2. \tag{13}$$

For $\mu_2 > 0$, we expect the amplitudes of A_s, A_i, and B to undergo first linear growth in the vicinity of the solution (8), and then to be saturated by nonlinear terms. The spatial scale at which these amplitudes develop is given by the inverse of the width of the band of unstable modes *i.e.* above threshold μ_c. As in case of lasers [5] for $\Omega < 0$, we have to choose the following multiple-scale expansions for t, x, and y:

$$\begin{cases} x = X_0 + \varepsilon X \\ y = Y_0 + \varepsilon Y \\ t = T_0 + \varepsilon T_1 + \varepsilon^2 T_2 + ... \end{cases} \tag{14}$$

Temporal and spatial derivatives in (9) are then replaced by

$$\begin{cases} \partial_t = \partial_{T_0} + \varepsilon\, \partial_{T_1} + \varepsilon^2\, \partial_{T_2} \\ \partial_x = \partial_{X_0} + \varepsilon\, \partial_X \\ \partial_y = \partial_{Y_0} + \varepsilon\, \partial_Y. \end{cases} \tag{15}$$

We now complete the specification of our model. The two parameters α_s and α_i are small. Therefore, the dynamics will depend on the relative magnitude of the small parameters involved in the problem, namely, ε, α_s, and α_i. Balance of the linear growth rates and walk-off in the asymptotic expansion imposes scaling relations between the small parameters ε, α_s, and α_i. This implies that $\alpha_s = O(\varepsilon)$ and $\alpha_i = O(\varepsilon)$. Therefore we may set

$$\begin{cases} \alpha_s = \varepsilon\, \widehat{\alpha}_s \\ \alpha_i = \varepsilon\, \widehat{\alpha}_i \end{cases} \tag{16}$$

where $\widehat{\alpha}_s = O(1)$ and $\widehat{\alpha}_i = O(1)$.
In the sequel the following compact notation for equations (9) is used

$$\partial_t V = LV + N \tag{17}$$

where the vector $V = (B, A_s, A_i^*)^T$ contains the field variables, L is the linear operator of the system:

(*See equation above*)

$$L_2 = \begin{pmatrix} i\gamma_p a_p(\partial_X^2+\partial_Y^2) & 0 & 0 \\ 0 & i\gamma_s a_s(\partial_X^2+\partial_Y^2) - \widehat{\alpha_s}\gamma_s\partial_X & \gamma_s\mu_2 \\ 0 & \gamma_i\mu_2 & -i\gamma_i a_i(\partial_X^2+\partial_Y^2) - \widehat{\alpha}_i\gamma_i\partial_X) \end{pmatrix}$$

and N is the nonlinear operator:

$$N = \begin{pmatrix} -\gamma_p\ A_s\ A_i \\ \gamma_s\ A_i^*\ B \\ \gamma_i\ A_s\ B^* \end{pmatrix}.$$

We emphasize here that N is the exact nonlinear term and does not result from a power expansion since the nonlinearity of the OPO is quadratic contrary to what is known in *e.g.* lasers.

The evolution equations for the field variables are classically obtained by expanding the solution V in power series of ε:

$$V = \varepsilon V^{(1)} + \varepsilon^2 V^{(2)} + \varepsilon^3 V^{(3)} + ... \tag{18}$$

The functions $V^{(i)}$ depend on the slow variables X, Y, T_1, and T_2. By substituting the expansion (18) and the relations (15) and (16) in (17), and then collecting coefficients of like powers of ε, the following equations are obtained

$$\begin{aligned} &(\partial_{T_0} - L_0)V^{(1)} = 0 && O(\varepsilon) \\ &(\partial_{T_0} - L_0)V^{(2)} = -\partial_{T_1}V^{(1)} + N_2 = G_2 && O(\varepsilon^2) \\ &(\partial_{T_0} - L_0)V^{(3)} = \\ &-\partial_{T_1}V^{(2)} + (-\partial T_2 + L_2)V^{(1)} + N_3 = G_3 && O(\varepsilon^3) \end{aligned} \tag{19}$$

where L_0 is the linear operator of the system for $\mu = \mu_c = \sqrt{1+\tilde{\Delta}^2}$, L_2 is defined by

(*See equation above*)

N_2 and N_3 are the nonlinear terms at $O(\varepsilon^2)$ and $O(\varepsilon^3)$.

At $O(\varepsilon)$ we find that:

$$V^{(1)} = \begin{pmatrix} 0 \\ 1 \\ \frac{(1+i\tilde{\Delta})}{\sqrt{1+\tilde{\Delta}^2}} \end{pmatrix} A(X,Y,T_1,T_2)\ e^{i\omega_c T_0}$$

where $\omega_c = \gamma_s\gamma_i(\Delta_i - \Delta_s)/(\gamma_s+\gamma_i)$.

The equations obtained from the coefficients of higher powers of ε are of the form: $(\partial_{T_0} - L_0)V^{(i)} = G_i$ for some right-hand side G_i, and the homogeneous equation at $O(\varepsilon)$ in (19) has a non trivial solution. Therefore, $V^{(i)}$ exists for $i > 1$ only if the terms G_i satisfy an appropriate solvability condition. It states that G_i must be orthogonal to the eigenvector $U = (0, \gamma_i\mu_c, \gamma_s(1-i\tilde{\Delta}))^T\ \exp i\omega_c T_0$ of the adjoint operator of $(\partial_{T_0} - L_0)$.

Applying the solvability condition at $O(\varepsilon^2)$ leads to:

$$\frac{\partial A}{\partial T_1} = 0. \tag{20}$$

The equation at $O(\varepsilon^2)$ in (19) has a solution

$$V^{(2)} = \begin{pmatrix} B_2 \\ 0 \\ 0 \end{pmatrix}$$

with

$$\begin{aligned} &B_2(X,Y,T_2) = \\ &-(1-\tilde{\Delta})(1-i\Delta_p)/\sqrt{(1+\Delta_p^2)(1+\tilde{\Delta}^2)}|A(X,Y,T_2)|^2. \end{aligned} \tag{21}$$

Similarly, applying the solvability condition at $O(\varepsilon^3)$ yields the form of an evolution equation:

$$\begin{aligned} \tau\partial_{T_2}A = &(c_r + ic_i)(\partial_X^2+\partial_Y^2)A + (\widehat{v}_g + i\widehat{w}_g)\partial_X A \\ &+(d_1+id_2)\mu_2 A - (N_1+iN_2)|A|^2 A \end{aligned} \tag{22}$$

where

$$\begin{aligned} \tau &= \frac{1}{\gamma_s\gamma_i}[(\gamma_s+\gamma_i)^2 + (\gamma_s-\gamma_i)^2\tilde{\Delta}^2] \\ c_r &= 2a\ \tilde{\Delta} > 0 \\ c_i &= (a_s-a_i)(\gamma_s+\gamma_i) - (a_s+a_i)(\gamma_s-\gamma_i)\tilde{\Delta}^2 \\ \widehat{\alpha} &= \gamma_s\ \widehat{\alpha}_s - \gamma_i\,\widehat{\alpha}_i \\ \widehat{v}_g &= (\gamma_s-\gamma_i)(\ \widehat{\alpha}_s - \ \widehat{\alpha}_i)\tilde{\Delta}^2 - (\gamma_s+\gamma_i)(\ \widehat{\alpha}_s + \ \widehat{\alpha}_i) \\ \widehat{w}_g &= 2\tilde{\Delta}\,\widehat{\alpha} \\ d_1 &= 2(1+\ \tilde{\Delta}^2)^{\frac{1}{2}}(\gamma_s+\gamma_i) \\ d_2 &= 2(1+\ \tilde{\Delta}^2)^{\frac{1}{2}}(\gamma_i-\gamma_s)\tilde{\Delta} \\ N_1 &= 2\frac{1-\tilde{\Delta}\Delta_p}{1+\Delta_p^2}(\gamma_s+\gamma_i) \\ N_2 &= 2\frac{1-\tilde{\Delta}\Delta_p}{1+\Delta_p^2}\tilde{\Delta}(\gamma_i-\gamma_s). \end{aligned}$$

In order to get a partial differential equation for A in terms of the original space and time variables, we use the total time and space derivatives of the signal amplitude given by $\partial_t A = \varepsilon^2\partial_{T_2}A$, $\partial_x A = \varepsilon\partial_X A$, $\partial_y A = \varepsilon\partial_Y A$, and the relations, $\mu = \mu_c + \varepsilon^2\mu_2$, $\alpha_s = \varepsilon\ \widehat{\alpha}_s$ and $\alpha_i = \varepsilon_i\,\widehat{\alpha}_i$. Note that (i) the fast variables T_0, X_0, and Y_0 do not appear in the total derivatives of the slowly varying amplitude A

because of the factorization of these variables, and (ii) the time scale T_1 disappears because of the solvability condition (20). Then we obtain after setting $\varepsilon A = A_1$:

$$\tau\partial_t A_1 = (c_r + ic_i)(\partial_x^2 + \partial_y^2)A_1 + (v_g + iw_g)\partial_x A_1 + (d_1 + id_2)(\mu - \mu_c)A_1 - (N_1 + iN_2)|A_1|^2 A_1 \quad (23)$$

where

$$v_g = (\gamma_s - \gamma_i)(\alpha_i - \alpha_s)\tilde{\Delta}^2 - (\gamma_s + \gamma_i)(\alpha_s + \alpha_i)$$
$$w_g = 2\tilde{\Delta}\alpha.$$

Before proceeding further in the analysis, it is instructive to get a physical interpretation of the different terms and their coefficients in equation (23). The parameter τ is the effective relaxation time for the mixing waves (signal and idler) and it reaches its minimum value when $\gamma_s = \gamma_i$. The parameters d_1 and d_2 are the weights, close to the instability threshold, of the growth rate and the frequency respectively. Let us remark that d_1 never vanishes and the threshold for instability is actually set by μ. On the contrary d_2 which acts only on the frequency vanishes when $\gamma_s = \gamma_i$.

The three remaining terms are of a great importance for our analysis. The diffraction coefficient c_i may also vanish for several situations and the obvious one is $a_s = a_i$ and $\gamma_s = \gamma_i$ while the diffusion coefficient c_r sets the limit of the validity of our reduced model for OPO systems. This coefficient is positive as it should be in order to avoid the spurious anti-diffusive instability, this is consistent with $\tilde{\Delta} > 0$ as considered in this paper. This condition can be fulfilled for OPOs in various situations except for Δ_s and Δ_i simultaneously negative. In fact, generally the presence of the diffusive term ($c_r > 0$) in optical systems where the original governing equations contain only diffraction terms stems from a non trivial interaction between diffraction, relaxation and dispersion as can be seen from the above definition of c_r. The origin of a similar diffusion term in an amplitude equation describing pattern formation in optical bistability was discussed in details by Le Berre *et al.* [21]. The nonlinear amplitude saturation coefficient N_1 depends on the sign of the quantity $1 - \tilde{\Delta}\Delta_P$, which we take positive in order to deal with a supercritical Hopf bifurcation. If $1 - \tilde{\Delta}\Delta_P < 0$ a subcritical Hopf bifurcation occurs with appearance of bistability [22]; saturation effects are then captured by quintic terms. This case requires a specific analysis and will be published later. On the opposite, the nonlinear phase modulation coefficient N_2 has no incidence on saturation effects and even vanishes for $\gamma_s = \gamma_i$. As expected the walk-off creates a first space derivative $\partial_x A_1$ with coefficients v_g and w_g. The presence of the term $iw_g\dfrac{\partial A_1}{\partial x}$ in equation (23) leads to an unusual form of the complex Ginzburg-Landau equation which deserves further processing to obtain a normal form amplitude equation. It has no equivalence in the other optical nonlinear systems as lasers, optical bistability, lasers with saturable absorber and Raman lasers for which classical Ginzburg-Landau or Swift-Hohenberg equations have been derived since the reflection symmetry ($x \to -x$) is preserved for all these systems. This gradient term is specific to OPO systems and characterizes the walk-off effect. Its physical importance will be understood in the light of the analysis of the linear version of equation (23).

Up to now, we have derived an evolution equation in presence of walk-off on the basis of the outcome of the stability analysis of the small deviations from the steady state solution (8) of the OPO equations. We are now going to proceed to a spatio-temporal stability analysis of the OPO off state solution (8) and the subsequent pattern formation.

4 Spatio-temporal instabilities

4.1 Brief survey of theory

We start this section by briefly recalling some ideas on convective and absolute instabilities. For the sake of simplicity, we state the results here for only one transverse spatial dimension (the wave vector $\mathbf{k} = (k_x, k_y)$ reduces to a wave number k), and the reader should consult reference [13] for details and reference [14] for generalizations to the bidimensional case.

To examine the stability of a basic state, we classically consider a wave packet $A_1(x,t) = \int_{-\infty}^{+\infty} a(k)e^{i(kx-\omega(k)t)}\,dk$ where $\omega = \omega(k)$ is the dispersion relation of the system. Using the method of steepest descent [23], it can be shown that the asymptotic form reached by the wave packet as $t \to \infty$ with $\dfrac{x}{t}$ bounded is:

$$A_1(x,t) \sim \frac{e^{i\left[\frac{x}{t}k-\omega(k)\right]t}}{\left[t\dfrac{d^2\omega}{dk^2}\right]^{\frac{1}{2}}}$$

where k is determined by $\dfrac{d\omega}{dk} = \dfrac{x}{t}$.

In case of temporal instability analysis, the system is unstable provided that $\mathrm{Im}(\omega) > 0$ for any *real* wave number, and the "most unstable" wave number k_c is defined by $\dfrac{d[\mathrm{Im}(\omega)]}{dk}|_{k=k_c} = 0$. The ray direction along which the maximum growth rate is reached is defined by $\dfrac{d[\mathrm{Re}(\omega)]}{dk}|_{k=k_c} = \dfrac{x}{t}$.

The second parameter domain of special interest concerning spatio-temporal instabilities, is that corresponding to a maximum growth rate for a given x as $t \to \infty$ that is $\dfrac{x}{t} \to 0$. The wave number associated with this instability satisfies the equation $\dfrac{d\omega}{dk}|_{k=k_0} = 0$, where k_0 must generally be *complex*.

Thus, a perturbation at fixed x grows with a rate $\mathrm{Im}[\omega(k_0)]$. When $\mathrm{Im}[\omega(k_0)]$ is positive, the system is said to be *absolutely unstable* (the absolute critical values are

denoted μ_{abs}, k_0, ω_{abs}). If $\mathrm{Im}[\omega(k_0)]$ is negative or equal to zero, $\mathrm{Im}[\omega(k_c)]$ being positive, the system is said to be *convectively unstable* (the values at threshold for convective instability are μ_{conv}, k_{conv}, ω_{conv}. Note that, in the absence of walk-off, $\mu_{abs} = \mu_{conv} = \mu_c$ where μ_c is defined at the end of Section 3.1 and corresponds to the usual instability threshold [4]). In the latter case, any localized perturbation is convected away so that instabilities cannot globally grow. In the former case (absolute instabilities) localized perturbations grow in situ and also expand in space. In the sequel, we show the interest of these ideas to describe spatio-temporal evolution of some unstable modes.

4.2 Walk-off introduces convective and absolute instabilities

As we are dealing with a 2D problem we seek solutions of the linearized version of equation (23) in the form $A_1 = \tilde{A}e^{i\omega t + i\,(k_x x + k_y y)}$. The broken reflection symmetry $x \to -x$, does not allow the emergence of coupled oblique traveling waves propagating in opposite directions. The dispersion equation is deduced from linearizing equation (23) and it reads

$$\omega = \frac{1}{\tau}[-k^2(c_i - ic_r) + k_x(v_g + iw_g) + (d_2 - id_1)(\mu - \mu_c)] \tag{24}$$

where $k^2 = k_x^2 + k_y^2$.

For ($\alpha_s = \alpha_i = 0$) we recover the standard solution of the OPO in the absence of walk-off, namely, a spatially homogeneous solution ($k_x^c = k_y^c = 0$) is found for $\mu = \mu_c$. When $\alpha \neq 0$, *i.e.* in the presence of walk-off, this bidimensional problem can be reduced to an equivalent one-dimensional problem, by means of Squire's transformation [24] as explained in the following. Squire's theorem states that if a Squire transformation can be found then the most unstable modes are unidimensional *i.e.* those which appear in the equivalent 1D problem. For this purpose we set:

$$\bar{v}_g \equiv \cos(\varphi)v_g, \quad \bar{w}_g \equiv \cos(\varphi)w_g \text{with}: \cos(\varphi) \equiv \frac{k_x}{k}$$
$$\bar{\mu} = \mu, \bar{\omega} = \omega. \tag{25}$$

Note that the transformation is not valid for $k_x = k_y = 0$.

The dispersion relation (24) is hereby reduced to the form:

$$\bar{\omega} = \frac{1}{\tau}[-k^2(c_i - ic_r) + k(\bar{v}_g + i\bar{w}_g) + (d_2 - id_1)(\bar{\mu} - \mu_c)]. \tag{26}$$

We solve the equivalent one-dimensional problem defined by (26). From the solution of this problem we can then derive the solution of the two-dimensional problem (24), by means of the transformation (25). Therefore the convective instability threshold is simply obtained by minimizing $\bar{\mu}$ with respect to the modulus k of the *real* wave vector $\mathbf{k} = (k_x, k_y)$ [24].

Hence, in the 1D problem (26) the critical value of k is determined by $\dfrac{d\bar{\mu}}{dk} = 0$ which leads to $\bar{\mu}_{conv}$, k_{conv} and $\bar{\omega}_{conv}$:

$$\bar{\mu}_{conv} = \mu_c - \frac{\bar{w}_g^2}{4c_r d_1} = \mu_c - \alpha^2 \frac{\Delta}{4a(\gamma_s+\gamma_i)^2\sqrt{1+\tilde{\Delta}^2}}\cos^2(\varphi)$$
$$k_{conv} = -\frac{\bar{w}_g}{2c_r} = -\frac{\alpha}{2a}\cos(\varphi)$$

and

$$\bar{\omega}_{conv} = -\frac{1}{\tau}\left(\frac{\tilde{\Delta}^2\alpha^2}{c_r^2}c_i + \frac{\tilde{\Delta}\alpha}{c_r^2}v_g + \frac{\tilde{\Delta}^2\alpha^2}{c_r^2 d_1}d_2\right)\cos^2(\varphi).$$

Taking into account transformation (25), the most unstable mode (*i.e.* that leads to the lowest value of $\bar{\mu}$) is obtained for $\varphi = 0$ giving rise to a solution in form of traveling waves propagating in the x direction at the onset of instability given by $\mu_{conv} = \mu_c - \alpha^2\Delta/\left[4a(\gamma_s+\gamma_i)^2\sqrt{1+\tilde{\Delta}^2}\right]$ with a *real* wave vector $k_x = k_{conv} = -\alpha/(2a)$ and $k_y = 0$.

Walk-off introduces a structure with a wave vector depending on the ratio of diffraction and walk-off parameters weighted by relaxation coefficients. Contrary to the threshold pump value which depends also on the effective detuning Δ, the wave vector at threshold is independent of Δ.

Squire's theorem also allows to obtain information on unstable oblique traveling waves which appear when μ exceeds the critical value μ_{conv} but is smaller than μ_c. In this sector unstable bidimensional structures may exist since $\varphi \neq 0$. As a result, the threshold for signal (and idler) emission can be lowered not only for transverse beams expanding in the walk-off direction but also for bidimensional beams (k_x and $k_y \neq 0$) according to the new instability region with respect to the standard (without walk-off) OPO which emerges between the curves $\mu = \mu_c - \alpha^2\Delta/\left[4a(\gamma_s+\gamma_i)^2\sqrt{1+\tilde{\Delta}^2}\right]$ and $\mu = \mu_c$. To summarize the presence of walk-off destabilizes the system and mostly forces the transverse beam to expand along the walk-off direction.

Once the specific role of the walk-off OPO "characteristic" term $iw_g\dfrac{\partial A_1}{\partial x}$ in the convective instability is clarified, it is interesting to describe the evolution of the instability in a frame moving with the group velocity of the most unstable mode. If we set $A_1 = \tilde{A}(x,y,t)e^{ik_{conv}x + i\omega_{conv}t}$, then the amplitude $\tilde{A}$ satisfies a complex Ginzburg-Landau equation in the form:

$$\tau\frac{\partial\tilde{A}}{\partial t} = (c_r + ic_i)\left(\frac{\partial^2}{\partial x^2} + \frac{\partial^2}{\partial y^2}\right)\tilde{A} + \left(\frac{c_i}{c_r}w_g + v_g\right)\frac{\partial\tilde{A}}{\partial x}$$
$$+ (d_1 + id_2)(\mu - \mu_{conv})\tilde{A} - (N_1 + iN_2)\tilde{A}|\tilde{A}|^2. \tag{27}$$

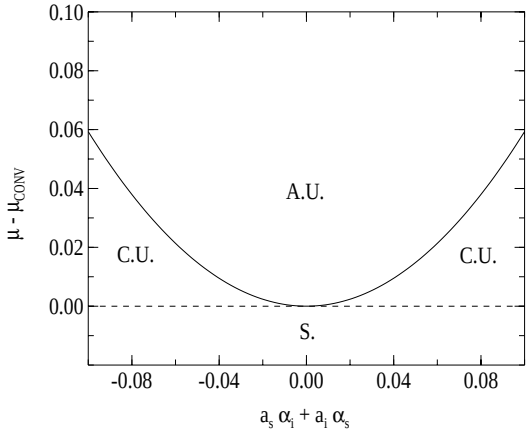

Fig. 3. Stability diagram of the OPO in presence of walk-off. The different types of instabilities are indicated on the figure. A.U, C.U., and S. stand for absolutely unstable, convectively unstable and linearly stable respectively.

Notice that, in the absence of walk-off, w_g and v_g vanish and the gradient term disappears in equation (27) leading to $\mu_{conv} = \mu_c$. Thus we recover the standard complex Ginzburg-Landau equation as it arises in many nonlinear studies of optical and fluid dynamical systems. In that case thresholds of linear, convective, and absolute instabilities coincide at the marginal instability giving rise directly to an absolute unstable regime. In the presence of walk-off, this order-parameter equation describes the growth of a travelling wave moving with the group velocity [25] $V_g = (\frac{c_i}{c_r} w_g + v_g)/\tau$ which is proportional to $a_i\alpha_s + a_s\alpha_i$. This parameter plays a central role in the nature of the emerging transverse patterns at threshold. Indeed, the walk-off does not allow for travelling waves moving in opposite directions as it may happen either in OPOs without walk-off [4] or in lasers [5]. This canonical form of Ginzburg-Landau equation with a gradient term has been extensively studied by Huerre and Monkewitz as a model of hydrodynamic resonances in separated shear flows [13]. They showed that this term is responsible for the gap between absolute and convective instabilities. For OPO systems, two striking features are already worthy to notice in the light of the above nonstandard Ginzburg-Landau equation. First, when $V_g = 0$, the first instability is absolute which means that no convective structures may occur in the OPO system. Second, for nonvanishing values of V_g either (i) $w_g \neq 0$ and the system undergoes a convective instability with an off-axis signal generation where $k_x = k_{conv} = -w_g/(2c_r)$, or (ii) $w_g = 0$ then the first instability still is convective but the generated signal is spatially homogeneous since $k_{conv} = 0$. The situation appears similar to that of standard OPOs (without walk-off) but the underlying difference in the nature of instabilities is of a great importance. The first instability is absolute for standard OPOs, however it is convective in presence of walk-off.

Figure 3 summarizes the different dynamical behaviors of the OPO in presence of walk-off. The OPO off state ($A_1 = 0$) is stable for $\mu - \mu_{conv} < 0$, convectively unstable for $\mu - \mu_{conv} > 0$, and below the curve; and absolutely unstable for values of $\mu - \mu_{conv}$ above the curve. Note that for $a_i\alpha_s + a_s\alpha_i = 0$ the thresholds for absolute and convective instabilities are degenerate and the system loses its stability by an absolute instability. For $a_i\alpha_s + a_s\alpha_i \neq 0$, there is a region of convective unstable regimes which expands as the parameter increases.

Let us now discuss the dynamics in the absolute and convective regimes. For $\mu > \mu_{conv}$, the OPO off state is convectively unstable if:

$$\mu_{conv} < \mu < \mu_{abs} =$$

$$\mu_{conv} + (a_i\alpha_s + a_s\alpha_i)^2 \frac{\tilde{\Delta}^2[(\gamma_s+\gamma_i)^2 + (\gamma_i-\gamma_s)^2\tilde{\Delta}^2]^2}{d_1 c_r(c_r^2+c_i^2)},$$

where μ_{abs} is the threshold for the absolute instability.

In this range, the response of the system to a localized perturbation grows continuously but it is simultaneously convected away, so that an observer at any fixed location sees the medium returning to the OPO off state. Therefore a continuous source of perturbations (noise) is required to sustain a permanent emitting state.

Whereas when $\mu > \mu_{abs}$, the OPO off state is absolutely unstable. The *complex* wave number k_0 at onset of absolute instability, is given by:

$$k_0 = \frac{v_g c_i - w_g c_r - 2i(a_i\alpha_s + a_s\alpha_i)\tilde{\Delta}\left[(\gamma_s+\gamma_i)^2 + (\gamma_i-\gamma_s)^2\tilde{\Delta}^2\right]}{2(c_i^2+c_r^2)}. \quad (28)$$

The excess gain with respect to threshold $\mu - \mu_{abs}$ rules the temporal evolution of the amplitude at any location. However, as can be seen from (28), spatial dynamics interferes with this amplification. Downstream ($x > 0$) spatial dynamics accelerates (for $a_i\alpha_s + a_s\alpha_i > 0$) the amplification, while upstream ($x < 0$) it attenuates this amplification but it is not strong enough to compensate for the temporal amplification. It results that, in the long time limit, the entire medium is contaminated by the response to any localized perturbation. In other words, the pattern expands transversely in both positive and negative x directions but the amplification is much faster downstream than upstream as it is checked numerically in the next section. Of course this spatio-temporal amplification is eventually saturated by nonlinearities. In these conditions the transverse pattern is generated from the self-dynamics of the system.

To summarize, in presence of walk-off, the OPO emerging transverse pattern at threshold may be either a noise-sustained or a self-sustained dynamical pattern depending on the value of the pump parameter with respect to the two instability thresholds μ_{conv} and μ_{abs}.

5 Numerical results

In this section we describe results of numerical simulations of the OPO complex nonstandard Ginzburg-Landau equation (Eq. (23)) above threshold, since it allows to check the onset of convective and absolute instabilities. In fact, the difficulty to handle mathematically the original theoretical model (Eq. (7)) leading to the lack of analytical results makes relevant the use of amplitude equations. Furthermore, it has often been checked that their validity qualitatively extends far beyond the instability threshold. For almost all OPO experimental situations, the transverse walk-off expansion is one dimensional which is also consistent with our bidimensional analytical study. Therefore, for the sake of simplicity and in accordance with our theoretical study, we have integrated equation (23) in 1D transverse coordinate (the walk-off direction coordinate x) by means of the split-step method. For each run we have set the length of the transverse interval of integration wide enough with respect to the width of localized structures to avoid numerical instabilities.

The most important result of our analysis is its ability to predict the spatio-temporal evolution of arbitrary initial perturbations corresponding to OPO practical situations. It comes out from the linear stability analysis that in the transient regime (linear system) OPOs can respond to a perturbation that is localized both in time and space in two qualitatively different ways; as discussed in the preceding section either a convective or an absolute instability develops. We only present here significant numerical simulations which have been performed with the pump gain parameter μ as a control parameter to check the different regimes and we have kept the signal and the idler walk-off to $\alpha_s = 0.4$ and $\alpha_i = 0.06$, respectively.

For all figures we have set the remaining parameters to $\gamma_p = \gamma_s = \gamma_i = 1$, $a_s = 0.2$, $a_i = 0.06$, $\Delta_p = -2$, $\Delta_s = 2$, and $\Delta_i = 2$, and the signal envelope has been initialized by a narrow Gaussian function at the origin (which also can approximate a Dirac distribution $\delta(x)$). The values of the parameters are the same as in reference [4] except for walk-off and diffraction parameters. We have chosen a large value for α_s with respect to α_i so that the signal field experiences a much larger walk-off effect than the idler field. This makes easier the qualitative comparison with the experimental situation considered in reference [8]. Notice that we have checked the analytical predictions for different values of α_s and α_i and we have observed that the walk-off effect decreases by decreasing the difference between α_s and α_i, in accordance with the definition of α in equations (12).

We first performed a series of numerical simulations in the transient (linear behavior) and asymptotic (nonlinear behavior) regimes, with OPO parameters close to but just above the convective instability threshold $\mu \gtrsim \mu_{conv}$. The spatio-temporal evolution of the signal envelope function $|A_1(x,t)|$ is illustrated in Figures 4 and 5 for μ just above the convective instability threshold (see Fig. 3). Two striking features are readily apparent in these plots. For small and intermediate values of time (Fig. 4a) a transient unstable wavepacket develops, travelling in the decreasing

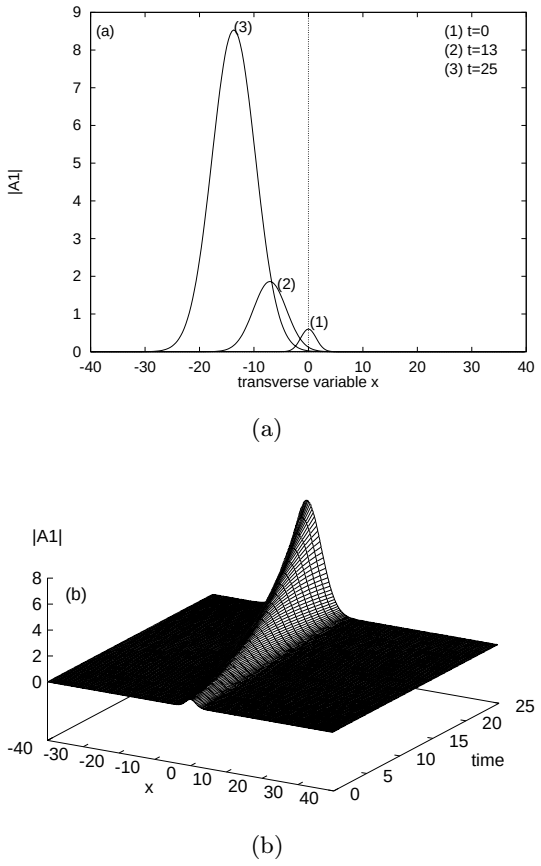

Fig. 4. Transient behavior in convective unstable regime. (a) Emergence of a convective transverse signal envelope just above the threshold of convective instability shown in Figure 3. The parameters are indicated in the text. Note both the growing and the propagation of the envelope. The signal envelope was initialized with a narrow transverse gaussian profile (the lower curve). (b) Convective spatio-temporal linear evolution of the signal envelope. The transverse profile expansion in the decreasing x direction is clear from the figure.

x direction as dictated by the convective linear instability characteristics. A three-dimensional plot representing the spatio-temporal evolution of the signal envelope is depicted in Figure 4b. The second striking feature is related to the role of the nonlinearity for long-time behavior. Saturation eventually dominates linear amplification as can be seen from Figure 5a. In this situation nonlinearity manifests itself only in saturation. The signal intensity grows, saturates, and propagates in the transverse direction but asymptotically returns to zero at a given x coordinate as shown in Figure 5b. The underlying convective character dominates the dynamics. In other words, the main consequence of the convective unstable regime is that the system acts as a spatial amplifier of localized fluctuations. At a fixed location, a local perturbation first grows with time and then decays as it is advected away. In a frame moving with the transverse group velocity, the perturbation is amplified and broadens. This phenomenon is also depicted

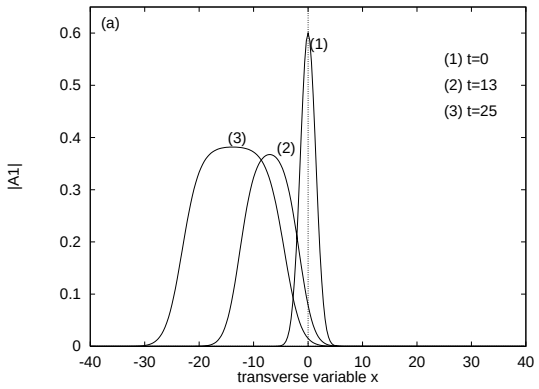

(a)

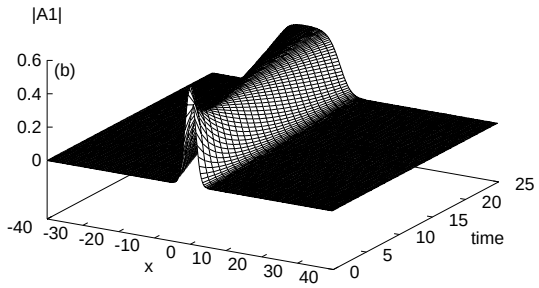

(b)

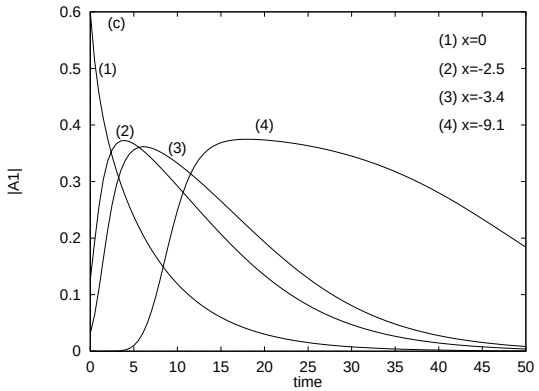

(c)

Fig. 5. Nonlinear saturation effects on the convective transverse envelope of the emerging signal of Figure 4. (a) Evolution at different times ($t = 0$, 13, 25). Notice that the envelope, at the origin, continuously decreases. (b) Spatio-temporal evolution of the signal envelope. Note that the effect of nonlinear terms is just to saturate the linear amplification. The convective character is always dominant. (c) Asymptotic behavior for 4 transverse locations of the envelope signal. The curves labelled (1), (2), (3) and (4) correspond to $x \simeq 0$, $x \simeq -2.5$, $x \simeq -3$, and $x \simeq -9$, respectively. The transverse domain acts as a spatial amplifier for incoming disturbances, but asymptotically all transverse locations vanish and the envelope returns to the ground state ($A_1 = 0$).

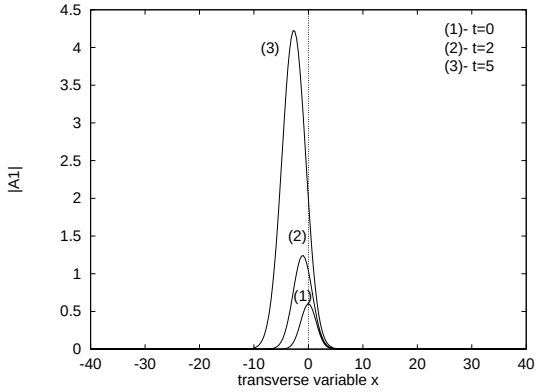

Fig. 6. Linear absolute temporal evolution of the transverse envelope of the signal, when the pump parameter is just above the limiting curve of convective instability (see Fig. 3). The remaining parameters are unchanged. Note the amplification in situ at the origin.

in Figure 5c where the temporal evolution of four transverse x locations are shown. At first ($t = 0$) the gaussian peak (maximum) is located at the origin and propagates in the decreasing x direction and the origin returns to the OPO off state after a transient as can be seen from the curve labelled (1) on Figure 5c. The three remaining curves represent the temporal evolution at the locations $x \simeq -2.5$ (curve (2)), $x \simeq -3.45$ (curve (3)), and $x \simeq -9$ (curve (4)). The perturbations grow as they are advected away and the system acts as a spatial amplifier of incoming perturbations. Ultimately, however, disturbances at a given location decay and $A_1 = 0$ (OPO off) is globally stable, even though the pump gain parameter μ exceeds the threshold value of classical linear instability. This spatio-temporal dynamics remains unchanged until the gain parameter μ crosses the critical curve delimiting the upper limit of the convective unstable zone, as discussed below.

When the pump gain parameter μ is further increased *i.e.* when $\mu > \mu_{abs}$ the system enters the absolute unstable zone. In order to illustrate the spatio-temporal evolution of the signal envelope in this region, which is quite different from the convective one, we have performed a second series of numerical simulations for a typical value of μ just above the absolute instability threshold. The main difference is that the leading and the trailing edges of the growing response to the localized initial condition, travel in opposite directions as shown in Figure 6 (compare to Fig. 4a). This behavior which is initiated in the transient regime is even reinforced by the saturation effects which are readily seen in Figure 7a for long-time evolution. The temporal evolution of the transverse distribution of the signal envelope is shown in Figure 7b where the saturated wave packet tends to invade the whole transverse domain. Contrarily to convective instability, at any transverse location perturbations are amplified and then saturate leading to a globally stable OPO on state. Figure 7c shows clearly the attracting state for the same transverse locations as in Figure 5c. Note the difference in the asymptotic states (OPO off and OPO on) of the system.

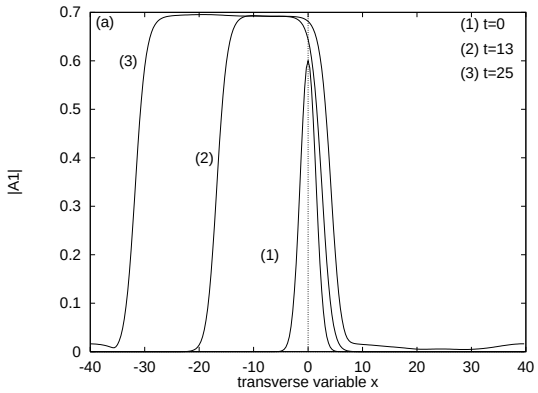

(a)

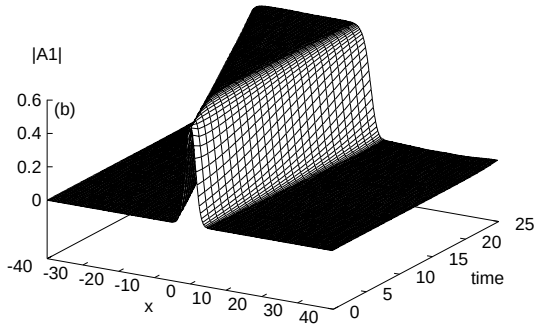

(b)

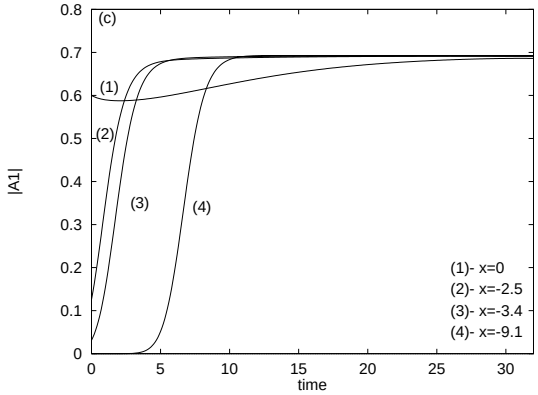

(c)

Fig. 7. Nonlinear absolute saturation of the envelope of Figure 6. (a) Temporal evolution for three selected times ($t = 0$, 13, 25) of the signal envelope built from a localized narrow gaussian initial beam. Note the amplitude amplification at the origin. (b) Spatio-temporal evolution of the transverse signal envelope. The transverse beam profile tends asymptotically to invade the whole spatial domain. (c) Asymptotic behavior of the envelope signal for 4 transverse locations . The curves labelled (1), (2), (3) and (4) correspond to $x \simeq 0$, $x \simeq -2.5$, $x \simeq -3$, and $x \simeq -9$ respectively. Contrarily to convective unstable regime (Fig. 5c), the transverse signal envelope bifurcates from the ground state ($A_1 = 0$) to a new state.

To end this section we would like to summarize the consequence of our analysis on the pattern formation in experimental OPO situations, in presence of walk-off. First, in case of positive effective detuning (Δ), and in the absence of walk-off, the generated signal, and idler, at threshold, are homogeneous and no pattern formation is expected. However, in the presence of walk-off, the main issue of our numerical and analytical analysis is that convective and absolute patterns may be observed in OPO experiments as they were observed in fluid mechanics [26]. Indeed the system becomes first convectively unstable and all fluctuations are carried out transversely even though the OPO off state is unstable. At the same time the system becomes very sensitive to permanent perturbations: if a noise source is applied, fluctuations are amplified (until nonlinear saturation occurs) and a pulse (localized structure) propagates in the decreasing or increasing x direction, depending on the sign of the "effective" walk-off. As a consequence a noise-sustained transverse signal is generated. These states disappear as soon as the noise is cancelled. This situation has been predicted and numerically checked, very recently by Santagiustina *et al.* [27] in a passive optical cavity filled by Kerr type nonlinear media when there is a tilt (the angle of incidence is not zero which is an equivalent to the walk-off angle) of the input pump beam. Above a second threshold, at larger values of the pump parameter, the system is absolutely unstable and noise does not play anymore an important role. Just above the onset of absolute instability an homogeneous solution builds up and, one may expect to observe self-sustained dynamical structures at even larger pump values.

6 Concluding remarks

In this paper we have carried out an analytical investigation of spatio-temporal dynamics of optical parametric oscillators in presence of diffraction and walk-off effects. Using Squire's theorem we found that the presence of walk-off destabilizes the OPO system and induces the formation of a transverse signal (idler) as a travelling wave expanding in the walk-off direction. This predicted behavior is qualitatively similar to that observed in recent experiments on OPOs [7,8] and in fluid convection [10].

We have also shown that beyond the threshold for signal and idler generation the spatio-temporal evolution of transverse patterns is described by a nonstandard (Eq. (23)) Ginzburg-Landau equation. Indeed, the walk-off introduces a new term responsible for the lowering of the threshold at the onset of instability on one hand, and for a gap between thresholds of convective and absolute instabilities on the other hand. Although we have carried out our study for a positive crystal, where the signal and idler are experiencing walk-off, and the pump is an ordinary beam, our analysis can easily be extended to all types of phase matching configurations. A spatio-temporal stability analysis permitted us to distinguish between the walk-off-induced convective and absolute

structures which may lead, in experimental OPO systems, to noise-sustained and/or self-sustained dynamical patterns. Two directions are of a major importance in extending the spatio-temporal dynamics of OPOs (in presence of walk-off). (i) We have limited the present work to the supercritical bifurcation case. If the bifurcation is subcritical, multistable states may occur in the system and nonlinear localized structures may have an important role in the transverse dynamics; for instance walk-off could induce 1D transverse structures of soliton type. (ii) For realistic OPO systems, the pump beam is spatially inhomogeneous. We have recently considered this situation in the laser problem [20,28], by means of absolute and convective instabilities. This spatio-temporal stability analysis appears as a powerful analytical method to deal with the presence of spatial inhomogeneities. Work in these directions is in progress.

The Laboratoire de Physique des Lasers, Atomes et Molécules is "Unité Mixte de Recherche du CNRS". The Centre d'Etudes et de Recherches Lasers et Applications (CERLA) is supported by the Ministère chargé de la Recherche, the Région Nord/Pas de Calais and the Fonds Européen de Développement Economique des Régions. We wish to thank C. Fabre, M. Le Berre, E. Ressayre and A. Tallet for useful discussions.

References

1. See *e.g.* A.P. Piskarskas, Opt. Photon. News, July 1997, 25; R.L. Byer, A.P. Piskarskas, feature issue on optical parametric oscillators, J. Opt. Soc. Am. B **10**, 1655 (1993).
2. R.L. Byer, *Optical parametric oscillators* in *Quantum Electronics*, edited by H. Rabin, C.L. Tang (Academic, New York, 1975).
3. C. Fabre, Phys. Rep. **219**, 215 (1992).
4. S. Longhi, Phys. Rev. A **53**, 4488 (1996).
5. J. Lega, P.K. Jacobsen, J.V. Moloney, A.C. Newell, Phys. Rev. A **49**, 4201 (1994).
6. M. Le Berre, D. Leduc, S. Patrascu, E. Ressayre, A. Tallet, *Beyond the mean-field model of the ring cavity*, private communication.
7. T. Nishikawa, N. Uesugi, Optics Comm. **124**, 512 (1996).
8. A.V. Smith, W.J. Alford, T.D. Raymond, M.S. Bowers, J. Opt. Soc. Am. B **12**, 2253 (1995).
9. T. Nishikawa, N. Uesugi, Optics Comm. **140**, 473 (1997).
10. M.T. Ouazzani, J.K. Platten, A. Mojtabi, Int. J. Heat Mass Transfer **33**, 1417 (1990).
11. H.W. Müller, M. Tveitereid, S. Trainoff, Phys. Rev. E **48**, 263 (1993).
12. F. Dufour, M.C. Neel, *Time-periodic convective patterns in a horizontal porous layer with through flow*, private communication.
13. P. Huerre, P.A. Monkewitz, Ann. Rev. Fluid. Mech. **22**, 473 (1990).
14. E. Infeld, G. Rowlands, *Nonlinear waves, solitons and chaos* (Cambridge University Press, 1990). See Chapter 3 and mainly Section 3.4 for bidimensional and higher dimension systems.
15. J.A. Fleck, M.D. Feit, J. Opt. Soc. Am. **73**, 920 (1983).
16. L.A. Lugiato, G.-L. Oppo, J.R. Tredicce, L.M. Narducci, M.A. Pernigo, J. Opt. Soc. Am. B **7**, 1019 (1990).
17. G.-L. Oppo, M. Brambilla, L.A. Lugiato, Phys. Rev. A **49**, 2028 (1994).
18. K. Staliunas, J. Mod. Opt. **42**, 1261 (1995).
19. K. Staliunas, Opt. Comm. **91**, 82 (1992).
20. M. Ouarzazi, P.A. Bois, M. Taki, Phys. Rev. A **53**, 4408 (1996).
21. M. Le Berre, E. Ressayre, A. Tallet, Quantum. Semiclass. Opt. **7**, 1 (1995).
22. C. Richy, K.I. Petstas, E. Giacobino, C. Fabre, L. Lugiato, J. Opt. Soc. Am. B **12**, 456 (1995).
23. C.M. Bender, S.A. Orszag, *Advanced Mathematical Methods for Scientists and Engineers* (McGraw-Hill international Editions, Mathematics series, New York, 1978).
24. P.G. Drazin, W.H. Reid, *Hydrodynamic Stability* (Cambridge University Press, Cambridge, 1981).
25. The gradient term involving V_g cannot be removed by a Galilean transformation since we are dealing with the response of the system to spatially localized initial conditions.
26. I. Vihinen, A.M. Honohan, S.P. Lin, Phys. Fluids **9**, 3117 (1997).
27. M. Santaguistina, P. Colet, M. San Miguel, D. Walgraef, Phys. Rev. Lett. **79**, 3633 (1997).
28. M. Taki, M.N. Ouarzazi, *2D-Localized Ginzburg-Landau structures in inhomogeneously pumped laser systems*, unpublished.